

# Geometric phase in plane-wave transmission by a dielectric structurally chiral slab with a central phase defect

Akhlesh Lakhtakia <sup>\*</sup>

Department of Engineering Science and Mechanics, The Pennsylvania State University, 1450 White Course Drive,  
University Park, Pennsylvania 16802, USA  
and School of Mathematics, University of Edinburgh, Edinburgh EH9 3FD, UK



(Received 17 February 2024; accepted 29 March 2024; published 17 April 2024)

A slab made of a dielectric structurally chiral medium (DSCM) strongly reflects the co-handed circularly polarized plane wave, but not the crosshanded circularly polarized plane wave, in a spectral regime called the circular Bragg regime. The effect of inserting a central phase defect in a DSCM slab with a modest number of structural periods is a spectral reflection hole in the circular Bragg regime, for co-handed incidence only. However, if the incident plane wave is left-circularly polarized, the geometric phase of the transmitted plane wave contains evidence of both the circular Bragg regime and the spectral reflection hole, regardless of the structural handedness of the DSCM. This evidence is indicative of the type of phase defect. The effect of inserting a central phase defect in a DSCM slab with a large number of structural periods is a spectral transmission hole in the circular Bragg regime, for crosshanded incidence only. The spectral transmission hole may be difficult to observe experimentally because of absorption inside the DSCM slab, but it will still be evident in the geometric phase of the transmitted plane wave, if the incident plane wave is left-circularly polarized.

DOI: [10.1103/PhysRevA.109.043517](https://doi.org/10.1103/PhysRevA.109.043517)

## I. INTRODUCTION

A rectilinearly propagating plane wave is partially reflected by and partially transmitted through a slab made of a homogeneous isotropic dielectric material. When that material is periodically nonhomogeneous in the thickness direction, the slab exhibits spectral regimes of high reflectance and correspondingly low transmittance, depending on the direction of propagation of the incident plane wave, provided the slab thickness is several periods [1,2]. The slab is often called a scalar Bragg grating and the high-reflectance spectral regimes are called the Bragg regimes (or zones). The focus of this paper is on the lowest-order Bragg regime.

When a central phase defect is inserted in a scalar Bragg grating, the (lowest-order) Bragg regime is punctured by a much narrower high-transmittance spectral regime, as demonstrated by Haus and Shank in 1976 [3]. This narrower regime is called a spectral reflection hole and is widely employed in laser optics [4] and optical-fiber communication [5,6]. Commonly, the central phase defect is a thin slab of a homogeneous dielectric material [7–9].

To realize a circular-polarization-sensitive spectral reflection hole, the slab must be made of a dielectric structurally chiral material (DSCM), exemplified by chiral sculptured thin films and chiral liquid crystals [10–15], and must be thick enough to have a moderate number of structural periods. In general, a DSCM slab discriminates between incident plane waves of different circular polarization states in the Bragg

regime. DSCMs and circularly polarized plane waves possess handedness. In the Bragg regime, the reflectance of a DSCM slab is very high for a co-handed incident plane wave, but not for the crosshanded one, leading to the term *circular Bragg regime* [16]. As the high reflectance in the circular Bragg regime is only for the co-handed incident plane wave, so is the spectral reflection hole arising from the insertion of a central phase defect in the DSCM slab.

Facile implementation of central phase defects in a DSCM slab is possible of the following two types.

(i) Layer defect: A homogeneous layer, whether isotropic [11] or anisotropic [12], of finite thickness is inserted in the center of the DSCM slab. The thickness and the constitutive parameter(s) of the homogeneous layer determine the center wavelength of the spectral reflection hole.

(ii) Twist defect: One half of the DSCM slab is twisted about the thickness axis with respect to the other half by a certain angle [13,15]. The twist angle determines the center wavelength of the spectral reflection hole. Needless to add, a twist defect is not possible with scalar Bragg gratings.

Examples of DSCMs with layer and twist defects are found in the bioworld as well [17,18].

Both types of phase defects may be combined to offer design flexibility [14,19]. DSCMs without a phase defect are attractive as relatively wideband optical filters [20–25], whereas DSCMs with a central phase defect are attractive as narrowband optical filters [13,26,27]. Both types of filters are also deployed for optical sensing [27–31] and lasing [32–35]. Notably, these applications are based on high or low values of reflectances and transmittances, which are all positive real numbers, but not on the reflection and transmission coefficients, which are complex numbers [36].

\*akhlesh@psu.edu

A quantity derivable from the transmission coefficients is the geometric phase [37–39]. This quantity is of current interest for research on chiral liquid crystals [40–43] and chiral sculptured thin films [44,45], with some potential for application [41,43,46]. The geometric-phase spectrum of plane-wave transmission through a DSCM slab contains a signature of the circular Bragg phenomenon, provided that the incident plane wave is not right-circularly polarized (RCP), whether the DSCM is structurally right handed or structurally left handed [45]. Furthermore, both the thickening of the DSCM slab and the reversal of structural handedness affect that geometric phase.

This paper is devoted to the signatures of central phase defects in the geometric-phase spectrum of the transmitted plane wave. The phase defect can be either (i) an anisotropic layer defect, (ii) a twist defect, or (iii) a combination of both defects. For calculations, the DSCM is taken to be a chiral sculptured thin film [47,48] and the anisotropic layer defect to be a columnar thin film [49]. Without significant loss of generality, both films are taken to be sequentially made by evaporating the same material in a vacuum chamber and the substrate is similarly oriented for the growth of both films, the only difference being that the substrate spins about a central normal axis passing through it when a chiral sculptured thin film is being grown but is stationary when a columnar thin film is being grown [36,49].

Parenthetically, if a structurally left-handed DSCM slab is interfaced with a structurally right-handed DSCM slab, both slabs being otherwise identical, the resulting structure exhibits the Bragg phenomenon for incident plane waves of both circular-polarization states [20,25,50] and may also guide surface waves [51,52]. However, a sudden change in structural handedness does not amount to a phase defect.

This paper is organized as follows. Section II provides the theoretical framework to calculate the geometric phase of the transmitted plane wave in relation to the incident plane wave. Numerical results are presented and discussed in Sec. III, and the paper ends with key conclusions in Sec. IV. An  $\exp(-i\omega t)$  dependence on time  $t$  is explicit, with  $\omega = 2\pi f$  as the angular frequency,  $f$  as the linear frequency, and  $i = \sqrt{-1}$ . With  $\varepsilon_0$  and  $\mu_0$ , respectively, denoting the permittivity and permeability of free space, the free-space wave number is denoted by  $k_0 = \omega\sqrt{\varepsilon_0\mu_0}$ ,  $\lambda_0 = 2\pi/k_0$  is the free-space wavelength, and  $\eta_0 = \sqrt{\mu_0/\varepsilon_0}$  is the intrinsic impedance of free space. The Cartesian coordinate system  $(x, y, z)$  is adopted. Vectors are in boldface and unit vectors are additionally decorated by a caret on top. Dyadics are double underlined. Column vectors are underlined and enclosed in square brackets. The asterisk (\*) denotes the complex conjugate, and the dagger ( $\dagger$ ) the conjugate transpose.

## II. THEORY

The DSCM slab with a central layer defect and a central twist defect occupies the region  $0 < z < L$ , where the regions  $0 < z < L_{\text{CSTF}} = 2N\Omega$  and  $L_{\text{CSTF}} + L_{\text{CTF}} < z < L = 2L_{\text{CSTF}} + L_{\text{CTF}}$  are occupied by a chiral sculptured thin film and the region  $L_{\text{CSTF}} < z < L_{\text{CSTF}} + L_{\text{CTF}}$  by a columnar thin film. Here,  $2\Omega$  is the period of the chiral sculptured thin film

along the  $z$  axis and  $N \in \{1, 2, 3, \dots\}$  is the number of periods on either side of the central phase defect.

### A. Relative permittivity dyadic

The relative permittivity dyadic of the dielectric matter in the region  $0 < z < L$  is given by

$$\underline{\underline{\varepsilon}}_{\text{rel}}(z) = \underline{\underline{S}}_z(h, p, \varphi, z) \cdot \underline{\underline{S}}_y(\chi) \cdot [\varepsilon_a \hat{\mathbf{z}}\hat{\mathbf{z}} + \varepsilon_b \hat{\mathbf{x}}\hat{\mathbf{x}} + \varepsilon_c \hat{\mathbf{y}}\hat{\mathbf{y}}] \cdot \underline{\underline{S}}_y^{-1}(\chi) \cdot \underline{\underline{S}}_z^{-1}(h, p, \varphi, z), \quad z \in (0, L). \quad (1)$$

The frequency-dependent relative permittivity scalars  $\varepsilon_a$ ,  $\varepsilon_b$ , and  $\varepsilon_c$  capture local orthorhombicity [36,49,53]. The tilt dyadic

$$\underline{\underline{S}}_y(\chi) = \hat{\mathbf{y}}\hat{\mathbf{y}} + (\hat{\mathbf{x}}\hat{\mathbf{x}} + \hat{\mathbf{z}}\hat{\mathbf{z}}) \cos \chi + (\hat{\mathbf{z}}\hat{\mathbf{x}} - \hat{\mathbf{x}}\hat{\mathbf{z}}) \sin \chi \quad (2)$$

contains  $\chi \in [0, \pi/2]$  as an angle of inclination with respect to the  $xy$  plane.

Both structural handedness and twist are captured by the rotation dyadic

$$\underline{\underline{S}}_z(h, p, \varphi, z) = \hat{\mathbf{z}}\hat{\mathbf{z}} + (\hat{\mathbf{x}}\hat{\mathbf{x}} + \hat{\mathbf{y}}\hat{\mathbf{y}}) \cos [h(\pi pz + \varphi)] + (\hat{\mathbf{y}}\hat{\mathbf{x}} - \hat{\mathbf{x}}\hat{\mathbf{y}}) \sin [h(\pi pz + \varphi)]. \quad (3)$$

Here,  $h \in \{-1, 1\}$  is the structural-handedness parameter, with  $h = -1$  for structural left-handedness and  $h = 1$  for structural right-handedness;  $p/2$  is the reciprocal of the period; and  $\varphi \in [0, 2\pi)$  is a twist about the  $z$  axis. The last two parameters are defined in piecewise fashion as follows:

$$p = \begin{cases} 1/\Omega & \\ 0 & \\ 1/\Omega & \end{cases}, \quad \varphi = \begin{cases} 0 & \\ 0 & \\ \varphi_t & \end{cases}, \quad z \in \begin{cases} (0, L_{\text{CSTF}}), \\ (L_{\text{CSTF}}, L_{\text{CSTF}} + L_{\text{CTF}}), \\ (L_{\text{CSTF}} + L_{\text{CTF}}, L). \end{cases} \quad (4)$$

The foregoing equations also apply for a chiral smectic liquid crystal containing a layer of a smectic liquid crystal [54,55]. Furthermore, the same equations can be used for a chiral nematic liquid crystal containing a layer of a nematic liquid crystal by setting  $\varepsilon_c = \varepsilon_a$  and  $\chi = 0$  [54]. It is also possible to specify  $\varepsilon_{a,b,c}$  and  $\chi$  in the defect layer differently from their respective values in the regions  $0 < z < L_{\text{CSTF}} = 2N\Omega$  and  $L_{\text{CSTF}} + L_{\text{CTF}} < z < L = 2L_{\text{CSTF}} + L_{\text{CTF}}$ , but that is not necessary for the present purpose.

### B. Boundary-value problem

The half-space  $z < 0$  is the region of incidence and reflection, while the half-space  $z > L$  is the region of transmission. A plane wave, propagating in the half-space  $z \leq 0$  at an angle  $\theta_{\text{inc}} \in [0, \pi/2)$  to the  $z$  axis and at an angle  $\psi \in [0, 2\pi)$  to the  $x$  axis in the  $xy$  plane, is incident on the chosen chiral sculptured thin film. The electric and magnetic field phasors associated with the incident plane wave are represented as [36]

$$\mathbf{E}^{\text{inc}}(\mathbf{r}) = \left[ \frac{(is - \mathbf{p}_+)}{\sqrt{2}} a_L - \frac{(is + \mathbf{p}_+)}{\sqrt{2}} a_R \right] \times \exp[ik(x \cos \psi + y \sin \psi)] \exp(ik_0 z \cos \theta_{\text{inc}}), \quad z < 0, \quad (5a)$$

and

$$\begin{aligned} \mathbf{H}^{\text{inc}}(\mathbf{r}) &= \frac{1}{i\eta_0} \left[ \frac{(is - \mathbf{p}_+)}{\sqrt{2}} a_L + \frac{(is + \mathbf{p}_+)}{\sqrt{2}} a_R \right] \\ &\times \exp[i\kappa(x \cos \psi + y \sin \psi)] \exp(ik_0 z \cos \theta_{\text{inc}}), \\ z &< 0, \end{aligned} \quad (5b)$$

where

$$\left. \begin{aligned} \kappa &= k_0 \sin \theta_{\text{inc}} \\ \mathbf{s} &= -\hat{\mathbf{x}} \sin \psi + \hat{\mathbf{y}} \cos \psi \\ \mathbf{p}_{\pm} &= \mp(\hat{\mathbf{x}} \cos \psi + \hat{\mathbf{y}} \sin \psi) \cos \theta_{\text{inc}} + \hat{\mathbf{z}} \sin \theta_{\text{inc}} \end{aligned} \right\}. \quad (6)$$

The amplitudes of the left-circularly polarized (LCP) and the RCP components of the incident plane wave, denoted by  $a_L$  and  $a_R$ , respectively, are assumed to be known.

The reflected electric and magnetic field phasors are expressed as

$$\begin{aligned} \mathbf{E}^{\text{ref}}(\mathbf{r}) &= - \left[ \frac{(is - \mathbf{p}_-)}{\sqrt{2}} r_L - \frac{(is + \mathbf{p}_-)}{\sqrt{2}} r_R \right] \\ &\times \exp[i\kappa(x \cos \psi + y \sin \psi)] \exp(-ik_0 z \cos \theta_{\text{inc}}), \\ z &< 0, \end{aligned} \quad (7a)$$

and

$$\begin{aligned} \mathbf{H}^{\text{ref}}(\mathbf{r}) &= - \frac{1}{i\eta_0} \left[ \frac{(is - \mathbf{p}_-)}{\sqrt{2}} r_L + \frac{(is + \mathbf{p}_-)}{\sqrt{2}} r_R \right] \\ &\times \exp[i\kappa(x \cos \psi + y \sin \psi)] \exp(-ik_0 z \cos \theta_{\text{inc}}), \\ z &< 0. \end{aligned} \quad (7b)$$

The transmitted electric and magnetic field phasors are represented as

$$\begin{aligned} \mathbf{E}^{\text{tr}}(\mathbf{r}) &= \left[ \frac{(is - \mathbf{p}_+)}{\sqrt{2}} t_L - \frac{(is + \mathbf{p}_+)}{\sqrt{2}} t_R \right] \\ &\times \exp[i\kappa(x \cos \psi + y \sin \psi)] \exp[ik_0(z-L) \cos \theta_{\text{inc}}], \\ z &> L, \end{aligned} \quad (8a)$$

and

$$\begin{aligned} \mathbf{H}^{\text{tr}}(\mathbf{r}) &= \frac{1}{i\eta_0} \left[ \frac{(is - \mathbf{p}_+)}{\sqrt{2}} t_L + \frac{(is + \mathbf{p}_+)}{\sqrt{2}} t_R \right] \\ &\times \exp[i\kappa(x \cos \psi + y \sin \psi)] \exp[ik_0(z-L) \cos \theta_{\text{inc}}], \\ z &> L. \end{aligned} \quad (8b)$$

The reflection amplitudes ( $r_L$  and  $r_R$ ) as well as the transmission amplitudes ( $t_L$  and  $t_R$ ) are unknown and require the solution of a boundary-value problem. Several numerical techniques exist to solve this problem [56–59]. The most straightforward technique requires the use of the piecewise uniform approximation of  $\underline{\underline{\epsilon}}_{\text{rel}}(z)$  followed by application of the  $4 \times 4$  transfer-matrix method [60]. The interested reader is referred to Ref. [36] for a detailed description of this technique.

Thereafter, the transmittance

$$T = \frac{|t_L|^2 + |t_R|^2}{|a_L|^2 + |a_R|^2} \in [0, 1] \quad (9)$$

can be calculated.

### C. Geometric phase

Any plane wave can be located on the Poincaré sphere using the polar angle  $\alpha \in [0, 2\pi)$  and the azimuthal angle  $\beta \in [-\pi/2, \pi/2]$ , and its Poincaré spinor can then be defined as

$$[\underline{\phi}] = \begin{bmatrix} \cos(\frac{\pi}{4} - \frac{\beta}{2}) \\ \sin(\frac{\pi}{4} - \frac{\beta}{2}) \exp(i\alpha) \end{bmatrix}. \quad (10)$$

The transmitted plane wave possesses the geometric phase

$$\Phi = \text{Arg}\{[\underline{\phi}^{\text{inc}}]^\dagger \cdot [\underline{\phi}^{\text{tr}}]\} \quad (11)$$

relative to the incident plane wave.

For an incident LCP plane wave,  $\alpha^{\text{inc}} = 0$  and  $\beta^{\text{inc}} = -\pi/2$  so that

$$[\underline{\phi}_L^{\text{inc}}] = \begin{bmatrix} 0 \\ 1 \end{bmatrix} \quad (12)$$

is the Poincaré spinor. For an incident RCP plane wave,  $\alpha^{\text{inc}} = 0$ ,  $\beta^{\text{inc}} = \pi/2$ , and

$$[\underline{\phi}_R^{\text{inc}}] = \begin{bmatrix} 1 \\ 0 \end{bmatrix} \quad (13)$$

is the Poincaré spinor.

The Stokes parameters of the transmitted plane wave are given by [61]

$$\left. \begin{aligned} s_0^{\text{tr}} &= |t_R|^2 + |t_L|^2 \\ s_1^{\text{tr}} &= 2 \text{Re}(t_L t_R^*) \\ s_2^{\text{tr}} &= 2 \text{Im}(t_L t_R^*) \\ s_3^{\text{tr}} &= |t_R|^2 - |t_L|^2 \end{aligned} \right\}. \quad (14)$$

Accordingly, the angles  $\alpha^{\text{tr}}$  and  $\beta^{\text{tr}}$  can be calculated using

$$\left. \begin{aligned} s_1^{\text{tr}} &= s_0^{\text{tr}} \cos \beta^{\text{tr}} \cos \alpha^{\text{tr}} \\ s_2^{\text{tr}} &= s_0^{\text{tr}} \cos \beta^{\text{tr}} \sin \alpha^{\text{tr}} \\ s_3^{\text{tr}} &= s_0^{\text{tr}} \sin \beta^{\text{tr}} \end{aligned} \right\}, \quad (15)$$

so that

$$[\underline{\phi}^{\text{tr}}] = \begin{bmatrix} \cos(\frac{\pi}{4} - \frac{\beta^{\text{tr}}}{2}) \\ \sin(\frac{\pi}{4} - \frac{\beta^{\text{tr}}}{2}) \exp(i\alpha^{\text{tr}}) \end{bmatrix} \quad (16)$$

is the Poincaré spinor of the transmitted plane wave. For later convenience, let  $\alpha_L^{\text{tr}}$ ,  $\beta_L^{\text{tr}}$ , and  $[\underline{\phi}_L^{\text{tr}}]$  refer to LCP incidence, whereas  $\alpha_R^{\text{tr}}$ ,  $\beta_R^{\text{tr}}$ , and  $[\underline{\phi}_R^{\text{tr}}]$  refer to RCP incidence.

### III. NUMERICAL RESULTS AND DISCUSSION

To use causal frequency-dependent constitutive parameters [62–64] for calculations, single-resonance Lorentzian functions were assumed for  $\epsilon_a$ ,  $\epsilon_b$ , and  $\epsilon_c$  as follows [53]:

$$\epsilon_{a,b,c}(\lambda_0) = 1 + \frac{p_{a,b,c}}{1 + (1/N_{a,b,c} - i\lambda_{a,b,c}/\lambda_0)^2}. \quad (17)$$

The oscillator strengths are determined by the values of  $p_{a,b,c}$ ,  $\lambda_{a,b,c}(1 + N_{a,b,c}^{-2})^{-1/2}$  are the resonance wavelengths, and  $\lambda_{a,b,c}/N_{a,b,c}$  are the resonance linewidths. The parameters used for most of the theoretical results reported here are as follows:  $p_a = 2.3$ ,  $p_b = 3.0$ ,  $p_c = 2.2$ ,  $\lambda_a = \lambda_c = 260$  nm,

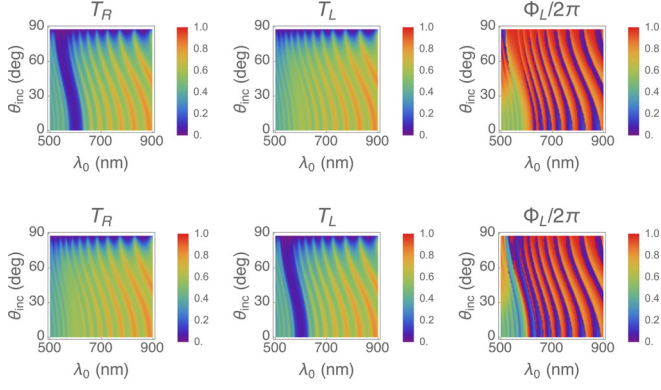


FIG. 1.  $T_R$ ,  $T_L$ , and  $\Phi_L$  as functions of  $\lambda_0$  and  $\theta_{\text{inc}}$  of a DSCM slab without a central phase defect ( $L_{\text{CTF}} = 0$  and  $\varphi_t = 0^\circ$ ), calculated for  $\psi = 0^\circ$ ,  $\Omega = 150$  nm, and  $N = 5$ . Other parameters are as follows:  $p_a = 2.3$ ,  $p_b = 3.0$ ,  $p_c = 2.2$ ,  $\lambda_a = \lambda_c = 260$  nm,  $\lambda_b = 270$  nm, and  $N_a = N_b = N_c = 130$ . Top row:  $h = 1$ . Bottom row:  $h = -1$ .

$\lambda_b = 270$  nm, and  $N_a = N_b = N_c = 130$ . Furthermore,  $\chi = 37^\circ$  and  $\Omega = 150$  nm were fixed.

Calculations of the transmittance  $T_R$  were made by setting  $a_R = 1$  and  $a_L = 0$ . Note that the corresponding geometric phase

$$\Phi_R = \text{Arg}\{[\phi_R^{\text{inc}}]^\dagger \cdot [\phi_R^{\text{tr}}]\} \equiv 0, \quad (18)$$

as shown elsewhere [44]. The transmittance  $T_L$  and the geometric phase  $\Phi_L = \alpha_L^{\text{tr}}$  were calculated by setting  $a_R = 0$  and  $a_L = 1$ .

### A. DSCM slab without central phase defect

For reference, Fig. 1 presents  $T_R$ ,  $T_L$ , and  $\Phi_L$  as functions of  $\lambda_0 \in [400 \text{ nm}, 900 \text{ nm}]$  and  $\theta_{\text{inc}} \in [0^\circ, 90^\circ]$  of a DSCM slab without a central phase defect ( $L_{\text{CTF}} = 0$  and  $\varphi_t = 0^\circ$ ), calculated for  $\psi = 0^\circ$ ,  $N = 5$ , and  $h = \pm 1$  [45]. The circular Bragg regime is evident as a blue trough in the plots of (i)  $T_R$  for  $h = 1$  and (ii)  $T_L$  for  $h = -1$ . The troughs are about 70-nm wide and centered at  $\lambda_0 \simeq 600$  nm for  $\theta_{\text{inc}} = 0^\circ$ ; they blueshift as  $\theta_{\text{inc}}$  increases, in accord with experimental results [65]. Although the two troughs look identical, they are somewhat different [45]. The blue trough is naturally absent in the plots of  $T_L$  for  $h = 1$  and  $T_R$  for  $h = -1$  [16].

Whereas  $\Phi_R \equiv 0$ , both plots of  $\Phi_L$  versus  $\lambda_0$  and  $\theta_{\text{inc}}$  in Fig. 1 contain a signature of the circular Bragg phenomenon. A reversal of structural handedness affects but does not lead to a simple change in  $\Phi_L$  [45].

### B. DSCM slab with a central twist defect

The introduction of a central  $90^\circ$  twist defect by itself is responsible for the insertion of a 15-nm-wide high-transmittance ridge in the center of the 70-nm-wide blue trough in the plots of (i)  $T_R$  versus  $\lambda_0 \in [400 \text{ nm}, 900 \text{ nm}]$  and  $\theta_{\text{inc}} \in [0^\circ, 90^\circ]$  for  $h = 1$  and (ii)  $T_L$  similarly for  $h = -1$ , as illustrated in Fig. 2 for  $\psi = 0^\circ$ . Like the troughs signifying the exhibition of the circular Bragg phenomenon, the high-transmittance ridges in both plots blueshift as  $\theta_{\text{inc}}$  increases. These ridges are spectral reflection holes.

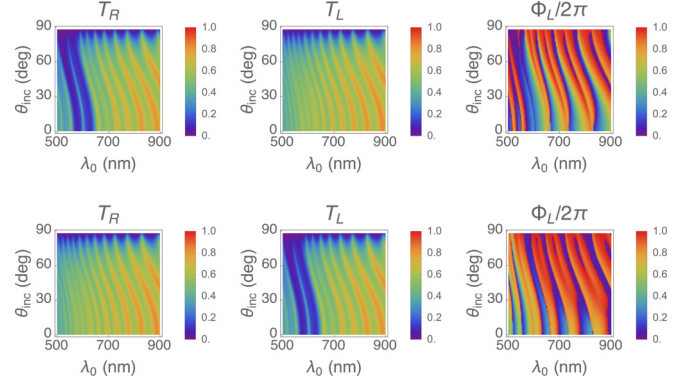


FIG. 2.  $T_R$ ,  $T_L$ , and  $\Phi_L$  as functions of  $\lambda_0$  and  $\theta_{\text{inc}}$  of a DSCM slab with a central twist defect ( $L_{\text{CTF}} = 0$  and  $\varphi_t = 90^\circ$ ), calculated for  $\psi = 0^\circ$ ,  $\Omega = 150$  nm, and  $N = 5$ . Other parameters are as follows:  $p_a = 2.3$ ,  $p_b = 3.0$ ,  $p_c = 2.2$ ,  $\lambda_a = \lambda_c = 260$  nm,  $\lambda_b = 270$  nm, and  $N_a = N_b = N_c = 130$ . Top row:  $h = 1$ . Bottom row:  $h = -1$ .

A linear feature right in the center of the circular Bragg regime also appears in the plots of  $\Phi_L$  versus  $\lambda_0$  and  $\theta_{\text{inc}}$  for  $h = \pm 1$  in Fig. 2, as a signature of the central twist defect. Additionally, the red-orange-yellow curvaceous ridges on the long-wavelength side of the circular Bragg regime in the plots of  $\Phi_L$  in Fig. 1 appear to have partially coalesced pairwise in the plots of  $\Phi_L$  in Fig. 2. The pairwise coalescence is partial because it is pronounced for low  $\theta_{\text{inc}}$  with bifurcation evident for high  $\theta_{\text{inc}}$ . Again, a reversal of structural handedness does not lead to a simple change in  $\Phi_L$  in Fig. 2.

Calculations (not shown here) indicate that the spectral reflection holes for  $h = \pm 1$  redshift within the circular Bragg regime when  $\varphi_t$  is progressively reduced from  $90^\circ$  to  $60^\circ$ , and they blueshift when  $\varphi_t$  is progressively increased from  $90^\circ$  to  $120^\circ$ .

### C. DSCM slab with a central layer defect

A central  $\Omega/4$ -thick layer defect alone is responsible for the insertion of a central 15-nm-wide high-transmittance ridge (i.e., spectral reflection hole) in the blue 70-nm-wide trough in the plots of (i)  $T_R$  for  $h = 1$  and (ii)  $T_L$  for  $h = -1$ , in Fig. 3. The high-transmittance ridges blueshift as  $\theta_{\text{inc}}$  increases, just as in Fig. 2.

A linear feature in the center of the circular Bragg regime and partial pairwise coalescence of curvaceous ridges on the long-wavelength side of the circular Bragg regime are also evident in the plots of  $\Phi_L$  versus  $\lambda_0$  and  $\theta_{\text{inc}}$  for  $h = \pm 1$  and  $\psi = 0^\circ$  in Fig. 3. However, visual comparison of Figs. 2 and 3 reveals that the effects of the central twist defect and the central layer defect on  $\Phi_L$  are quantitatively not identical.

The spectral reflection holes blueshift within the circular Bragg regime when  $L_{\text{CTF}}$  is progressively reduced from  $\Omega/2$  to  $\Omega/3$ , and redshift when  $L_{\text{CTF}}$  is progressively increased from  $\Omega/2$  to  $2\Omega/3$ , according to calculations not reported here in detail.

### D. DSCM slab with central layer and twist defects

Both types of central phase defects can cooperate to generate spectral reflection holes [14]. Therefore, for  $L_{\text{CTF}} = \Omega/4$

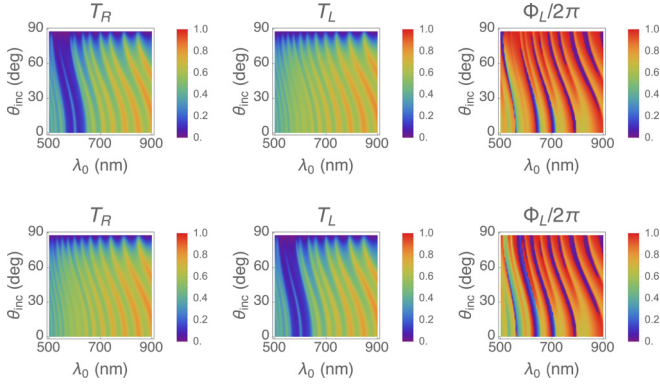


FIG. 3.  $T_R$ ,  $T_L$ , and  $\Phi_L$  as functions of  $\lambda_0$  and  $\theta_{\text{inc}}$  of a DSCM slab with a central layer defect ( $L_{\text{CTF}} = \Omega/2$  and  $\varphi_t = 0^\circ$ ), calculated for  $\psi = 0^\circ$ ,  $\Omega = 150$  nm, and  $N = 5$ . Other parameters are as follows:  $p_a = 2.3$ ,  $p_b = 3.0$ ,  $p_c = 2.2$ ,  $\lambda_a = \lambda_c = 260$  nm,  $\lambda_b = 270$  nm, and  $N_a = N_b = N_c = 130$ . Top row:  $h = 1$ . Bottom row:  $h = -1$ .

and  $\varphi_t = 135^\circ$ , a central 15-nm-wide high-transmittance ridge is present in the center of the blue 70-nm-wide trough in the plots in Fig. 4 of (i)  $T_R$  versus  $\lambda_0$  and  $\theta_{\text{inc}}$  for  $h = 1$  and (ii)  $T_L$ , also versus  $\lambda_0$  and  $\theta_{\text{inc}}$ , for  $h = -1$ . More importantly in the present context, a linear feature manifests as a signature of the combined defects in the plots of  $\Phi_L$  versus  $\lambda_0$  and  $\theta_{\text{inc}}$  for  $h = \pm 1$ , in that figure. The two defects also combine to effect the partial pairwise coalescence of curvaceous ridges on the long-wavelength side of the circular Bragg regime.

Figures 1–4 show the spectrums of  $T_R$ ,  $T_L$ , and  $\Phi_L$  for  $\theta_{\text{inc}} \in [0^\circ, 90^\circ]$  with  $\psi = 0^\circ$  fixed. Both  $T_R$  and  $T_L$  for DSCM slabs without central phase defects have long been known to vary weakly with  $\psi$  [36]. In contrast, it was recently shown [45] that  $\Phi_L$  does depend significantly on  $\psi$  for a defect-free DSCM slab (i.e.,  $L_{\text{CTF}} = 0$  and  $\varphi_t = 0^\circ$ ), as confirmed by Fig. 1.

Figure 5 presents  $T_R$ ,  $T_L$ , and  $\Phi_L$  as functions of  $\lambda_0 \in [400$  nm, 900 nm] and  $\psi \in [0^\circ, 360^\circ]$  for a DSCM slab with central layer and twist defects, when  $\theta_{\text{inc}} = 0^\circ$ . Clearly,  $T_R$  and

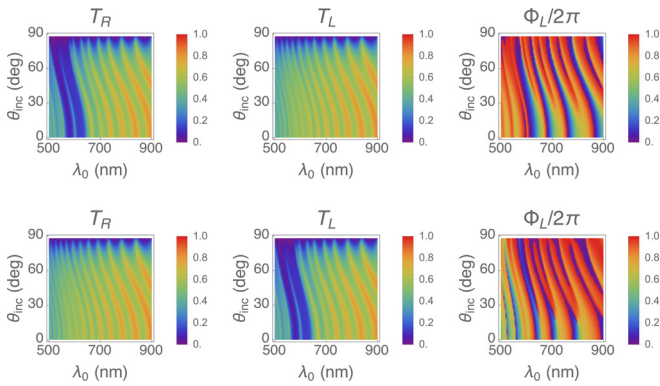


FIG. 4.  $T_R$ ,  $T_L$ , and  $\Phi_L$  as functions of  $\lambda_0$  and  $\theta_{\text{inc}}$  of a DSCM slab with central layer and twist defects ( $L_{\text{CTF}} = \Omega/4$  and  $\varphi_t = 135^\circ$ ), calculated for  $\psi = 0^\circ$ ,  $\Omega = 150$  nm, and  $N = 5$ . Other parameters are as follows:  $p_a = 2.3$ ,  $p_b = 3.0$ ,  $p_c = 2.2$ ,  $\lambda_a = \lambda_c = 260$  nm,  $\lambda_b = 270$  nm, and  $N_a = N_b = N_c = 130$ . Top row:  $h = 1$ . Bottom row:  $h = -1$ .

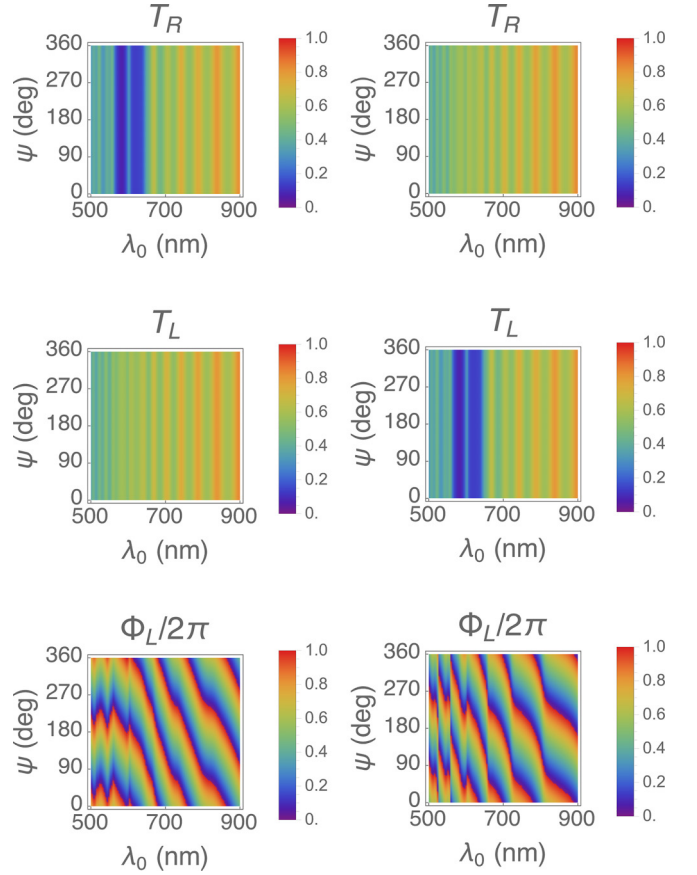


FIG. 5.  $T_R$ ,  $T_L$ , and  $\Phi_L$  as functions of  $\lambda_0$  and  $\psi$  of a DSCM slab with central layer and twist defects ( $L_{\text{CTF}} = \Omega/4$  and  $\varphi_t = 135^\circ$ ), calculated for  $\theta_{\text{inc}} = 0^\circ$ ,  $\Omega = 150$  nm, and  $N = 5$ . Other parameters are as follows:  $p_a = 2.3$ ,  $p_b = 3.0$ ,  $p_c = 2.2$ ,  $\lambda_a = \lambda_c = 260$  nm,  $\lambda_b = 270$  nm, and  $N_a = N_b = N_c = 130$ . Left column:  $h = 1$ . Right column:  $h = -1$ .

$T_L$  depend very weakly on  $\psi$ , whether in or out of the circular Bragg regime; and even the spectral reflection hole varies very little with  $\psi$ . Although the spectral reflection hole is clearly evident as a vertical feature in the plots of  $\Phi_L$ , that quantity depends strongly on  $\psi$  inside as well as outside the circular Bragg regime.

Although transmittance data for  $\psi \in [180^\circ, 360^\circ]$  can be obtained from transmittance data for  $\psi \in [0^\circ, 180^\circ]$  by exploiting symmetry, the same cannot be said for geometric-phase data. Linearity permits the representation

$$\left. \begin{aligned} t_L &= t_{LL} a_L + t_{LR} a_R \\ t_R &= t_{RL} a_L + t_{RR} a_R \end{aligned} \right\}, \quad (19)$$

so that  $T_L = |t_{LL}|^2 + |t_{RL}|^2$  and  $T_R = |t_{RR}|^2 + |t_{LR}|^2$ . Examination of the calculated data reveals that

$$\left. \begin{aligned} t_{LL}(h, \theta_{\text{inc}}, \psi) &= t_{RR}(-h, \theta_{\text{inc}}, 2\pi - \psi) \\ t_{LR}(h, \theta_{\text{inc}}, \psi) &= t_{RL}(-h, \theta_{\text{inc}}, 2\pi - \psi) \\ t_{RL}(h, \theta_{\text{inc}}, \psi) &= t_{LR}(-h, \theta_{\text{inc}}, 2\pi - \psi) \\ t_{RR}(h, \theta_{\text{inc}}, \psi) &= t_{LL}(-h, \theta_{\text{inc}}, 2\pi - \psi) \end{aligned} \right\}. \quad (20)$$

These symmetries imply that

$$\left. \begin{aligned} T_L(h, \theta_{\text{inc}}, \psi) &= T_R(-h, \theta_{\text{inc}}, 2\pi - \psi) \\ T_R(h, \theta_{\text{inc}}, \psi) &= T_L(-h, \theta_{\text{inc}}, 2\pi - \psi) \end{aligned} \right\} \quad (21)$$

so that the transmittances for  $\{h, \psi\}$  can be obtained from the transmittances for  $\{-h, 2\pi - \psi\}$ . However, the symmetries

$$\left. \begin{aligned} \alpha_L^{\text{tr}}(h, \theta_{\text{inc}}, \psi) &= 2\pi - \alpha_R^{\text{tr}}(-h, \theta_{\text{inc}}, 2\pi - \psi) \\ \alpha_R^{\text{tr}}(h, \theta_{\text{inc}}, \psi) &= 2\pi - \alpha_L^{\text{tr}}(-h, \theta_{\text{inc}}, 2\pi - \psi) \end{aligned} \right\} \quad (22)$$

and

$$\left. \begin{aligned} \beta_L^{\text{tr}}(h, \theta_{\text{inc}}, \psi) &= -\beta_R^{\text{tr}}(-h, \theta_{\text{inc}}, 2\pi - \psi) \\ \beta_R^{\text{tr}}(h, \theta_{\text{inc}}, \psi) &= -\beta_L^{\text{tr}}(-h, \theta_{\text{inc}}, 2\pi - \psi) \end{aligned} \right\} \quad (23)$$

which also stem from Eqs. (20), are unfruitful for a similar exercise with geometric phases because  $\Phi_R \equiv 0$  but  $\Phi_L$  can be nonzero.

By choosing  $L_{\text{CTF}}$  and  $\varphi_t$  appropriately, the spectral reflection holes can be positioned anywhere inside the circular regime. For example, when  $\theta_{\text{inc}} = \psi = 0$ , these features are located at  $\lambda_0 \approx 610$  nm when  $L_{\text{CTF}} = 0.4\Omega$  and  $\varphi_t = 120^\circ$  (results not shown), instead of at  $\lambda_0 \approx 600$  nm when  $L_{\text{CTF}} = 0.5\Omega$  and  $\varphi_t = 135^\circ$  (Fig. 5).

### E. Crossover to spectral transmission holes

Both types of central phase defects can engender, singly [66–68] as well as jointly [19,69], spectral transmission holes, when  $N$  is sufficiently large. A remarkable crossover, from

(1) a spectral reflection hole in the response of a structurally right-handed ( $h = 1$ ) and non-dissipative DSCM slab with a central  $90^\circ$  twist defect to a normally incident (i.e.,  $\theta_{\text{inc}} = 0$ ) RCP plane wave [13] to

(2) a spectral transmission hole in the response of the same slab to a normally incident LCP plane wave, with increasing  $N$ , emerged from theoretical analysis [66].

Theory shows the analogous crossover, from

(1) a spectral reflection hole in the response of a structurally left-handed ( $h = -1$ ) and nondissipative DSCM slab with a central  $90^\circ$  twist defect to a normally incident (i.e.,  $\theta_{\text{inc}} = 0$ ) LCP plane wave to

(2) a spectral transmission hole in the response of the same slab to a normally incident RCP plane wave, with increasing  $N$ . The spectral reflection hole is considerably wider than the spectral transmission hole, as explained by coupled-mode theory [68]. That approximate theory, however, has not yielded the crossover value of  $N$  [68].

Figure 6 is the counterpart of Fig. 4, the first drawn for  $N = 25$  and the second for  $N = 5$ . The reflection hole in the spectrum of  $T_R$  (or  $T_L$ ) for  $h = 1$  (or  $h = -1$ ) in Fig. 4 has been replaced by a much narrower transmission hole in the spectrum of  $T_L$  (or  $T_R$ ) for  $h = 1$  (or  $h = -1$ ) in Fig. 6, whether the plane wave is incident normally or obliquely.

Although the ultranarrow spectral transmission hole is clearly present in the plots of  $\Phi_L$ , it is hard to recognize it in the transmittance spectrums in Fig. 6 because the much thicker DSCM slab absorbs electromagnetic radiation very

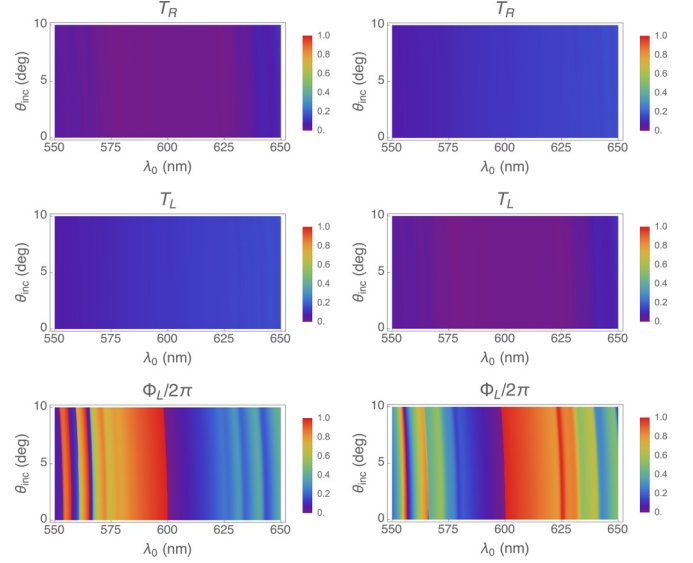


FIG. 6.  $T_R$ ,  $T_L$ , and  $\Phi_L$  as functions of  $\lambda_0$  and  $\theta_{\text{inc}}$  of a DSCM slab with central layer and twist defects ( $L_{\text{CTF}} = \Omega/4$  and  $\varphi_t = 135^\circ$ ), calculated for  $\psi = 0^\circ$ ,  $\Omega = 150$  nm, and  $N = 25$ . Other parameters are as follows:  $p_a = 2.3$ ,  $p_b = 3.0$ ,  $p_c = 2.2$ ,  $\lambda_a = \lambda_c = 260$  nm,  $\lambda_b = 270$  nm, and  $N_a = N_b = N_c = 130$ . Left column:  $h = 1$ . Right column:  $h = -1$ .

well. When the dissipation in the DSCM was reduced by setting  $\lambda_a = \lambda_b = \lambda_c = 10$  nm and calculations were carried out for  $N = 25$ , the resulting plot of  $T_L$  (or  $T_R$ ) for  $h = 1$  (or  $h = -1$ ) in Fig. 7 shows the spectral transmission hole very well.

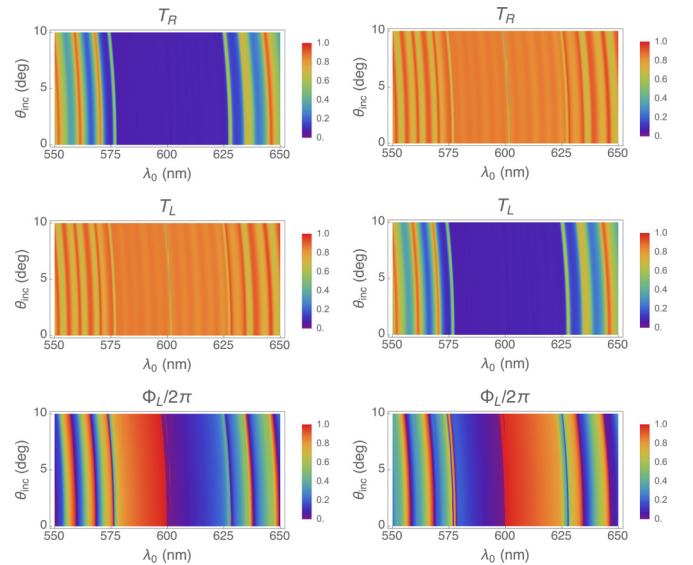


FIG. 7.  $T_R$ ,  $T_L$ , and  $\Phi_L$  as functions of  $\lambda_0$  and  $\theta_{\text{inc}}$  of a DSCM slab with central layer and twist defects ( $L_{\text{CTF}} = \Omega/4$  and  $\varphi_t = 135^\circ$ ), calculated for  $\psi = 0^\circ$ ,  $\Omega = 162$  nm, and  $N = 25$ . Other parameters are as follows:  $p_a = 2.3$ ,  $p_b = 3.0$ ,  $p_c = 2.2$ ,  $\lambda_a = \lambda_b = \lambda_c = 10$  nm, and  $N_a = N_b = N_c = 130$ . Left column:  $h = 1$ . Right column:  $h = -1$ .

#### IV. CONCLUDING REMARKS

The effect of inserting a central phase defect in a DSCM slab with a modest number of structural periods is the emergence of a narrowband high-transmittance feature (i.e., a spectral reflection hole) in the circular Bragg regime, only when the handedness of the incident circularly polarized plane wave is the same as the structural handedness of the DSCM. However, regardless of the structural handedness of the DSCM, the geometric phase of the transmitted plane wave contains evidence of both the circular Bragg regime and the spectral reflection hole, if the incident plane wave is LCP. The geometric phase of the transmitted plane wave is identically zero, if the incident plane wave is RCP.

A comparison of Figs. 2–4 indicates that the spectral reflection holes due to a central twist defect, a central layer defect, or a combined defect in a DSCM slab manifest in the same way in the transmittance plots. However, the geometric-phase signatures of both types of defects and of their combination are all different. Thus, the type of central phase defect could conceivably be gleaned by determining  $\Phi_L$  as a function of  $\lambda_0$  and  $\theta_{\text{inc}}$ , possibly using machine-learning techniques [70,71].

When the DSCM slab with the central phase defect is thick enough to have a large number of the structural periods, the narrow-band high-transmittance feature in the response

to an incident co-handed circularly polarized plane wave is replaced by an ultra-narrow-band high-reflectance feature in the response to an incident cross-handed circularly polarized plane wave. The new feature may be difficult to observe experimentally because of absorption inside the DSCM slab, but it will still be evident in the geometric phase of the transmitted plane wave, if the incident plane wave is LCP.

Spatial variation of the geometric phase on the multi-wavelength scale has been used for optical applications [41,46,72–75]. In the same vein, coating of curved surfaces of transparent objects by DSCMs, with and without central phase defects and even with multiple phase defects, is envisaged for circular-polarization-state-discriminatory [39] lensing applications. Instead of curved surfaces, surfaces decorated by multi-wavelength-sized planar facets could also be used, as also surfaces decorated with arrays of metasurfaces. These avenues are promising because both cholesteric liquid crystals [41,42,75] and chiral sculptured thin films [76–78] can be deposited on nonplanar surfaces.

#### ACKNOWLEDGMENT

The author thanks the Charles Godfrey Binder Endowment at Penn State for continued support of his research.

- 
- [1] W. L. Bragg, *Proc. Cambr. Philos. Soc.* **17**, 43 (1913).
  - [2] P. P. Ewald, *Ann. Phys. (Leipzig)* **354**, 117 (1916).
  - [3] H. A. Haus and C. V. Shank, *IEEE J. Quantum Electron.* **12**, 532 (1976).
  - [4] G. P. Agrawal and N. K. Dutta, *Semiconductor Lasers* (Van Nostrand Reinhold, New York, 1993).
  - [5] G. P. Agrawal and S. Radic, *IEEE Photon. Technol. Lett.* **6**, 995 (1994).
  - [6] F. Bakhti and P. Sansonetti, *J. Lightwave Technol.* **15**, 1433 (1997).
  - [7] R. Marz, *Integrated Optics: Design and Modeling* (Artech House, Boston, 1995).
  - [8] K. Iizuka, *Elements of Photonics* (Wiley, New York, 2002).
  - [9] P. W. Baumeister, *Optical Coating Technology* (SPIE, Bellingham, WA, 2004).
  - [10] A. Lakhtakia and M. McCall, *Opt. Commun.* **168**, 457 (1999).
  - [11] I. J. Hodgkinson, Q. h. Wu, A. Lakhtakia, and M. W. McCall, *Opt. Commun.* **177**, 79 (2000).
  - [12] A. Lakhtakia, V. C. Venugopal, and M. W. McCall, *Opt. Commun.* **177**, 57 (2000).
  - [13] I. J. Hodgkinson, Q. h. Wu, K. E. Thorn, A. Lakhtakia, and M. W. McCall, *Opt. Commun.* **184**, 57 (2000).
  - [14] S. Y. Vetrov, M. V. Pyatnov, and I. V. Timofeev, *Phys. Rev. E* **90**, 032505 (2014).
  - [15] M. V. Pyatnov, S. Y. Vetrov, and I. V. Timofeev, *Phys. Rev. E* **97**, 032703 (2018).
  - [16] M. Faryad and A. Lakhtakia, *Adv. Opt. Photon.* **6**, 225 (2014).
  - [17] A. Mendoza Galván, K. Järrendahl, and H. Arwin, *J. Vac. Sci. Technol. B* **37**, 062904 (2019).
  - [18] I. E. Carter, K. Weir, M. W. McCall, and A. R. Parker, *J. R. Soc. Interface* **13**, 20160015 (2016).
  - [19] I. J. Hodgkinson, Q. h. Wu, L. De Silva, M. Arnold, M. W. McCall, and A. Lakhtakia, *Phys. Rev. Lett.* **91**, 223903 (2003).
  - [20] J. Adams, W. Haas, and J. Dalley, *J. Appl. Phys.* **42**, 4096 (1971).
  - [21] S. D. Jacobs, K. A. Cerqua, K. L. Marshall, A. Schmid, M. J. Guardalben, and K. J. Skerrett, *J. Opt. Soc. Am. B* **5**, 1962 (1988).
  - [22] Y. J. Park, K. M. A. Sobahan, and C. K. Hwangbo, *Opt. Express* **16**, 5186 (2008).
  - [23] Y. Huang, M. Jin, and S. Zhang, *Jpn. J. Appl. Phys.* **53**, 072601 (2014).
  - [24] D. Chen, X.-B. Yin, Y.-J. Liu, L.-L. Zhang, J. Ma, and W.-M. Sun, *Chin. Phys. Lett.* **32**, 074208 (2015).
  - [25] R. A. Fiallo, M. W. Horn, and A. Lakhtakia, *J. Opt. Soc. Am. B* **39**, 2697 (2022).
  - [26] S. M. Pursel, M. W. Horn, and A. Lakhtakia, *Opt. Eng.* **46**, 040507 (2007).
  - [27] S. M. Pursel and M. W. Horn, *J. Vac. Sci. Technol. B* **25**, 2611 (2007).
  - [28] A. Lakhtakia, M. W. McCall, J. A. Sherwin, Q. H. Wu, and I. J. Hodgkinson, *Opt. Commun.* **194**, 33 (2001).
  - [29] Y. J. Liu, J. Shi, F. Zhang, H. Liang, J. Xu, A. Lakhtakia, S. J. Fonash, and T. J. Huang, *Sens. Actuat. B: Chem.* **156**, 593 (2011).
  - [30] S. H. Lee, D. P. Singh, J. H. Sung, M.-H. Jo, K. C. Kwon, S. Y. Kim, H. W. Jang, and J. K. Kim, *Sci. Rep.* **6**, 19580 (2016).
  - [31] C.-W. Chen and I. C. Khoo, *Proc. Natl. Acad. Sci. USA* **118**, e2021304118 (2021).
  - [32] J. Schmidtke, W. Stille, and H. Finkelmann, *Phys. Rev. Lett.* **90**, 083902 (2003).
  - [33] A. D. Ford, S. M. Morris, and H. J. Coles, *Mater. Today* **9**, 36 (2006).

- [34] P. Palffy-Muhoray, W. Cao, M. Moreira, B. Taheri, and A. Munoz, *Philos. Trans. R. Soc. A* **364**, 2747 (2006).
- [35] R. D. M. Topf and M. W. McCall, *Phys. Rev. A* **90**, 053824 (2014).
- [36] A. Lakhtakia and R. Messier, *Sculptured Thin Films: Nano-engineered Morphology and Optics* (SPIE, Bellingham, WA, 2003).
- [37] S. Pancharatnam, *Proc. Indian Acad. Sci. A* **44**, 247 (1956).
- [38] R. Bhandari, *Curr. Sci. (India)* **67**, 224 (1994).
- [39] R. Bhandari, *Phys. Rep.* **281**, 1 (1997).
- [40] R. Barboza, U. Bortolozzo, M. G. Clerc, and S. Residori, *Phys. Rev. Lett.* **117**, 053903 (2016).
- [41] M. Rafayelyan and E. Brasselet, *Opt. Lett.* **41**, 3972 (2016).
- [42] J. Kobashi, H. Yoshida, and M. Ozaki, *Nat. Photon.* **10**, 389 (2016).
- [43] P. Chen, B.-Y. Wei, W. Hu, and Y.-Q. Lu, *Adv. Mater.* **32**, 1903665 (2020).
- [44] A. Das, S. Mandal, R. A. Fiallo, M. W. Horn, A. Lakhtakia, and M. Pradhan, *J. Opt. Soc. Am. B* **40**, 2418 (2023); Replace “tan” by “sin” in Eq. (5b).
- [45] A. Lakhtakia, *J. Opt. Soc. Am. B* **41**, 500 (2024).
- [46] C. P. Jisha, S. Nolte, and A. Alberucci, *Laser Photon. Rev.* **15**, 2100003 (2021).
- [47] N. O. Young and J. Kowal, *Nature (London)* **183**, 104 (1959).
- [48] K. Robbie, M. J. Brett, and A. Lakhtakia, *Nature (London)* **384**, 616 (1996).
- [49] I. J. Hodgkinson and Q. h. Wu, *Birefringent Thin Films and Polarizing Elements* (World Scientific, Singapore, 1997).
- [50] A. Lakhtakia and I. J. Hodgkinson, *Opt. Commun.* **167**, 191 (1999).
- [51] J. Gao, A. Lakhtakia, and M. Lei, *Phys. Rev. A* **81**, 013801 (2010).
- [52] J. Gao, A. Lakhtakia, and M. Lei, *J. Nanophoton.* **5**, 051502 (2011).
- [53] C. Kittel, *Introduction to Solid State Physics* (Wiley Eastern, New Delhi, 1974).
- [54] P. G. de Gennes and J. Prost, *The Physics of Liquid Crystals*, 2nd ed. (Clarendon Press, Oxford, 1993).
- [55] O. Parodi, *J. Phys. Colloq.* **36**, C1-325 (1975).
- [56] R. Dreher and G. Meier, *Phys. Rev. A* **8**, 1616 (1973).
- [57] A. Sugita, H. Takezoe, Y. Ouchi, A. Fukuda, E. Kuze, and N. Goto, *Jpn. J. Appl. Phys.* **21**, 1543 (1982).
- [58] C. Oldano, E. Miraldi, and P. Taverna Valabrega, *Phys. Rev. A* **27**, 3291 (1983).
- [59] A. Lakhtakia and W. S. Weiglhofer, *Proc. R. Soc. London A* **453**, 93 (1997).
- [60] T. G. Mackay and A. Lakhtakia, *The Transfer-Matrix Method in Electromagnetics and Optics* (Morgan & Claypool, San Ramon, CA, 2020).
- [61] J. D. Jackson, *Classical Electrodynamics*, 3rd ed. (Wiley, New York, 1999).
- [62] M. Frisch, *Brit. J. Phil. Sci.* **60**, 459 (2009).
- [63] H. Silva and B. Gross, *Phys. Rev.* **60**, 684 (1941).
- [64] P. Kinsler, *Eur. J. Phys.* **32**, 1687 (2011).
- [65] S. Erten, A. Lakhtakia, and G. D. Barber, *J. Opt. Soc. Am. A* **32**, 764 (2015).
- [66] V. I. Kopp and A. Z. Genack, *Phys. Rev. Lett.* **89**, 033901 (2002).
- [67] M. Becchi, S. Ponti, J. A. Reyes, and C. Oldano, *Phys. Rev. B* **70**, 033103 (2004).
- [68] F. Wang and A. Lakhtakia, *Proc. R. Soc. Lond. A* **461**, 2985 (2005).
- [69] J. Schmidtke and W. Stille, *Eur. Phys. J. E* **12**, 553 (2003).
- [70] C. M. Bishop, *Pattern Recognition and Machine Learning* (Springer, New York, 2006).
- [71] P. Fieguth, *An Introduction to Pattern Recognition and Machine Learning* (Springer, Cham, Switzerland, 2022).
- [72] Z. Bomzon, G. Biener, V. Kleiner, and E. Hasman, *Opt. Lett.* **27**, 1141 (2002).
- [73] L. Marrucci, E. Karimi, S. Slussarenko, B. Piccirillo, E. Santamato, E. Nagali, and F. Sciarrino, *J. Opt. (Bristol)* **13**, 064001 (2011).
- [74] Y. Li, J. Kim, and M. J. Escuti, *Proc. SPIE* **8274**, 827415 (2012).
- [75] L. Zhu, C.-T. Xu, P. Chen, Y.-H. Zhang, S.-J. Liu, Q.-M. Chen, S.-J. Ge, W. Hu, and Y.-Q. Lu, *Light: Sci. Appl.* **11**, 135 (2022).
- [76] Y.-P. Zhao, D.-X. Ye, G.-C. Wang, and T.-M. Lu, *Nano Lett.* **2**, 351 (2002).
- [77] M. W. Horn, M. D. Pickett, R. Messier, and A. Lakhtakia, *Nanotechnology* **15**, 303 (2004).
- [78] R. A. Fiallo, C. Li, A. Lakhtakia, and M. W. Horn, *J. Nanophoton.* **17**, 036005 (2023).